

Lorentz-noninvariant neutrino oscillations: model and predictions

Frans R. Klinkhamer

Institut für Theoretische Physik,
Universität Karlsruhe (TH),
76128 Karlsruhe, Germany

Abstract

We present a three-parameter model for three flavors of massless left-handed neutrinos with Fermi-point splitting and trimaximal mixing angles. One of these parameters is the T -violating phase β , for which the experimental results from K2K and KamLAND appear to favor a nonzero value. In this article, we give further model predictions for neutrino oscillations. Future experiments, in particular MINOS, will be able to test this simple model. Possible implications for proposed experiments and neutrino factories are discussed.

PACS numbers: 14.60.St, 11.30.Cp, 73.43.Nq

Keywords: Non-standard-model neutrinos, Lorentz noninvariance, Quantum phase transition

Electronic address: frans.klinkhamer@physik.uni-karlsruhe.de

I. INTRODUCTION

Several experiments of the last few years [1, 2, 3, 4, 5, 6, 7, 8, 9] have presented (indirect) evidence for neutrino oscillations over a large enough travel distance, $L > 100 \text{ km}$. No evidence for neutrino oscillations has been seen at $L < 1 \text{ km}$ [10, 11].

The standard explanation for neutrino oscillations invokes the mass-difference mechanism; see, e.g., Refs. [12, 13, 14, 15, 16] and two recent reviews [17, 18]. Another possibility, based on an analogy with condensed-matter physics [19], is the Fermi-point-splitting mechanism suggested by Volovik and the present author. The idea is that a quantum phase transition could give rise to Lorentz noninvariance and CPT violation via the splitting of a multiply degenerate Fermi point; see Ref. [20] for a brief introduction and Ref. [21] for the details. Regardless of the origin, it may be worthwhile to study modifications of the neutrino dispersion law other than mass terms, Fermi-point splitting being one of the simplest such modifications.

A first comparison of this Lorentz-noninvariant mechanism for neutrino oscillations with the current experimental data from K2K and KamLAND (with input from SK) was presented in Ref. [22]. Rough agreement was found for a two-parameter model with trimaximal mixing angles. The comparison with the experimental data also showed a preference for a nonzero T (violating phase).

In this article, we give further details and try to make predictions for possible future experiments, e.g., MINOS [23, 24], JPARC [25, 26], BNL [27], beta beams [28], neutrino factories [29, 30], and reactor experiments [31]. These new experiments could easily falsify a simple three-parameter model with trimaximal mixing (a direct extension of the previous two-parameter model) or even the basic idea of the Fermi-point-splitting mechanism (which, in the absence of small additional mass terms, predicts undistorted energy spectra).

The outline of this article is as follows. In Section II, we discuss the general form of the dispersion law with Fermi-point splitting. In Section III, we present a simple three-parameter model for three flavors of massless left-handed neutrinos with Fermi-point splitting and trimaximal mixing angles. In Section IV, we calculate the neutrino oscillation probabilities for the model considered. In Section V, we obtain preliminary values for the three parameters of the model and make both general and specific predictions (the latter are for MINOS and JPARC (SK) in particular). In Section VI, we sketch a few scenarios of what future neutrino-oscillation experiments could tell us about the relevance of the Fermi-point-splitting model.

II. FERM I-POINT-SPLITTING ANSATZ

In the limit of vanishing Yukawa couplings, the Standard Model fermions are massless Weyl fermions, which have the following dispersion law:

$$E_{a,f}(q)^2 = c_f^2 q^2 + b_{0a}^{(f)^2}; \quad (2.1)$$

for three-momentum \mathbf{q} and with $b_{0a}^{(f)} = 0$ for the momentum. Here, a labels the sixteen types of massless left-handed Weyl fermions in the Standard Model (with a hypothetical left-handed antineutrino included) and f distinguishes the three known fermion families. For right-handed Weyl fermions and the same parameters, the plus sign inside the square on the right-hand side of Eq. (2.1) becomes a minus sign; cf. Refs. [21, 32].

The Weyl fermions of the original Standard Model have all $b_{0a}^{(f)}$ in Eq. (2.1) vanishing, which makes for a multiply degenerate Fermi point $\mathbf{q} = 0$. [Fermi points (gap nodes) \mathbf{q}_n are points in three-dimensional momentum space at which the energy spectrum $E(\mathbf{q})$ of the fermionic quasi-particle has a zero, i.e., $E(\mathbf{q}_n) = 0$.]

Negative parameters $b_{0a}^{(f)}$ in the dispersion law (2.1) split this multiply degenerate Fermi point into Fermi surfaces. [Fermi surfaces S_n are two-dimensional surfaces in three-dimensional momentum space on which the energy spectrum $E(\mathbf{q})$ is zero, i.e., $E(\mathbf{q}) = 0$ for all $\mathbf{q} \in S_n$.] Positive parameters $b_{0a}^{(f)}$ make the respective Fermi points disappear altogether (the energy being larger than zero for all momenta). See Refs. [20, 21] for a discussion of the physics that could be responsible for Fermi-point splitting. Note that the dispersion law (2.1) with nonzero parameters $b_{0a}^{(f)}$ selects a class of preferred reference frames [32, 33, 34].

Possible effects of Fermi-point splitting include neutrino oscillations [21, 22], as long as the neutrinos are not too much affected by the mechanism of mass generation. The hope is that massless (or nearly massless) neutrinos provide a window on "new physics" for which Lorentz invariance is an emergent phenomenon [19]. Let us, then, turn to the phenomenology of massless neutrinos with Fermi-point splittings.

We start from the observation that the Fermi-point splittings of the Standard Model fermions may have a special pattern tracing back to the underlying physics, just as happens for the so-called {phase of spin-triplet pairing in superconductors [20, 21]. As an example, we consider the following factorized Ansatz for the timelike splittings of Fermi points [21]:

$$b_{0a}^{(f)} = Y_a b_0^{(f)} ; \text{ for } a = 1; \dots; 16; f = 1; 2; 3 ; \quad (2.2)$$

Given the hypercharge values Y_a of the Standard Model fermions, there is only one arbitrary energy scale b_0 per family. The motivation of the particular choice (2.2) is that the induced electromagnetic Chern-Simons-like term cancels out exactly (the result is directly related to the absence of perturbative gauge anomalies in the Standard Model). This cancellation mechanism allows for b_0 values much larger than the experimental upper limit on the Chern-Simons energy scale, which is of the order of 10^{33} eV [34]. Other radiative effects from nonzero b_0 remain to be calculated; cf. Ref. [35].

The dispersion law of a massless left-handed neutrino (hypercharge $Y_L = -1$) is now given by

$$E_{L,f}(\mathbf{q})^2 = c^2 |\mathbf{q}|^2 + b_0^{(f)2} ; \quad (2.3)$$

with $f = 1; 2; 3$; for three neutrinos. The corresponding right-handed antineutrino ($Y_R = 1$)

is taken to have the following dispersion law :

$$E_{R,f}(q)^2 = c^2 |q|^2 + b_0^{(f)^2}; \quad (2.4)$$

with $\epsilon = 1$. Starting from Dirac fermions the natural choice would be $\epsilon = 1/2$ [1, 32], but, in the absence of a definitive mechanism for the Fermi-point splitting, we keep both possibilities open. [We do not consider the further generalization of having ϵ in Eq. (2.4) depend on the family index f .]

The parameters $b_0^{(f)}$ in these dispersion laws act as chemical potentials. This may be compared to the role of rest mass in a generalized dispersion law :

$$E(q)^2 = c^2 |q|^2 + b_0^2 + m^2 c^4 = c^2 |q|^2 + b_0^2 + \frac{m^2 c^4}{2c^2 |q|^2}; \quad (2.5)$$

for $|q| \gg \max(|b_0|, mc)$. The energy change from a nonzero b_0 always dominates the effect from $m c^2$ for large enough momenta $|q|$. In order to search for Fermi-point splitting, it is therefore preferable to use neutrino beams with the highest possible energy.

III. THREE-PARAMETER NEUTRINO MODEL

Now define three flavor states $\bar{\nu}_i, \nu_i, \bar{\nu}_i^c$ in terms of the left-handed propagation states $\bar{\nu}_i, \nu_i, \bar{\nu}_i^c$, which have dispersion law (2.3) with parameters $b_0^{(f)}$, $f = 1, 2, 3$. With a unitary 3×3 matrix U , the relation between these states is

$$\begin{pmatrix} \bar{\nu}_1 \\ \bar{\nu}_2 \\ \bar{\nu}_3 \end{pmatrix} = U \begin{pmatrix} \bar{\nu}_1^c \\ \bar{\nu}_2^c \\ \bar{\nu}_3^c \end{pmatrix}; \quad (3.1)$$

The matrix U can be parametrized [17, 18] by one phase, $\delta \in [0, 2\pi]$, and three mixing angles, $\theta_{12}, \theta_{13}, \theta_{23} \in [0, \pi/2]$:

$$U = \begin{pmatrix} \cos\theta_{12}\cos\theta_{13} & \sin\theta_{12}\cos\theta_{13} & \sin\theta_{13}e^{i\delta} \\ -\sin\theta_{12}\cos\theta_{13} & \cos\theta_{12}\cos\theta_{13} & 0 \\ \sin\theta_{13}e^{-i\delta} & 0 & \cos\theta_{13} \end{pmatrix} \begin{pmatrix} \bar{\nu}_1^c \\ \bar{\nu}_2^c \\ \bar{\nu}_3^c \end{pmatrix}; \quad (3.2)$$

using the standard notation s_x and c_x for $\sin x$ and $\cos x$.

In this article, we generalize the Ansatz of Ref. [22] by allowing for unequal ($\neq 1$) energy steps b_0 between the first and second families and between the second and third. Specially, we introduce the parameters

$$B_0 = b_0^{(2)} - b_0^{(1)}; \quad (3.3a)$$

$$r = b_0^{(3)} - b_0^{(2)} = B_0; \quad (3.3b)$$

which are assumed to be nonnegative. The overall energy scale of the three shifts $b_0^{(f)}$ is left undetermined. Note, however, that positive $b_0^{(f)}$ in Eq. (2.3) give rise to topologically-protected Fermi surfaces; cf. Refs. [19, 21].

The mixing angles are again taken to be trimaximal [22],

$$\theta_{13} = \arctan \frac{p}{1+2} = 5^\circ; \quad (3.4a)$$

$$\theta_{21} = \theta_{32} = \arctan 1 = 45^\circ; \quad (3.4b)$$

These particular values maximize, for given phase δ , the following T {violation (CP {nonconservation) measure [36]:

$$J = \frac{1}{8} \cos \theta_{13} \sin 2\theta_{13} \sin 2\theta_{21} \sin 2\theta_{32} \sin \delta; \quad (3.5)$$

In one of the first articles on neutrino oscillations, Bilenky and Pontecorvo [13] already emphasized the essential difference between leptons and quarks, where the latter have quantum numbers which are conserved by the strong interactions. They argued that, for two flavors, the only natural value of the neutrino mixing angle is 0 or 45° . But, at this moment, we do not know of a physical mechanism that convincingly explains the trimaximal values (3.4) and we simply use these values as a working hypothesis.

In short, the model (3.1)-(3.4), for dispersion law (2.3), has three parameters: the fundamental energy-difference scale B_0 , the ratio r of the consecutive energy steps, and the T {violating phase δ . This model will be called the "simple" Fermi-point-splitting model in the following (a more general Fermi-point-splitting model would have arbitrary mixing angles).

IV. OSCILLATION PROBABILITIES

The calculation of neutrino oscillation probabilities is technically straightforward but conceptually rather subtle; cf. Refs [14, 15, 16]. We, therefore, consider a stationary monoenergetic beam of left-handed neutrinos originating from a specified interaction region and propagating over a distance L to a suitable detector. That is, the neutrinos start out with a definite flavor (here, labeled $A; B; C$) and have a spread in their momenta due to the Heisenberg uncertainty principle ($\Delta x_m \Delta p_n \sim \hbar$).

With the dispersion law (2.3) and large enough neutrino energy ($E \gg \max [b_0^{(f)}]$), the trimaximal model of the previous section gives the following neutrino oscillation probabilities:

$$\begin{aligned}
P(A \rightarrow B) &= \frac{2^h}{9} \sin^2 \frac{21}{2} + 1 + \frac{p}{3} \frac{\bar{c}}{c} \sin^2 \frac{31}{2} + 1 + \frac{p}{3} \frac{\bar{c}}{c} \sin^2 \frac{32}{2} \\
&\quad + (1=2) \frac{p}{3} \frac{\bar{s}}{s} \sin \theta_{21} \sin \theta_{31} + \sin \theta_{32} ; \\
P(A \rightarrow C) &= \frac{2^h}{9} \sin^2 \frac{21}{2} + 1 + \frac{p}{3} \frac{\bar{c}}{c} \sin^2 \frac{31}{2} + 1 + \frac{p}{3} \frac{\bar{c}}{c} \sin^2 \frac{32}{2} \\
&\quad + (1=2) \frac{p}{3} \frac{\bar{s}}{s} \sin \theta_{21} \sin \theta_{31} + \sin \theta_{32} ; \\
P(A \rightarrow A) &= 1 - P(A \rightarrow B) - P(A \rightarrow C); \\
P(B \rightarrow C) &= \frac{2^h}{9} (1=2) \frac{\bar{s}}{s} \sin^2 \frac{21}{2} + \sin^2 \frac{31}{2} + \sin^2 \frac{32}{2} \\
&\quad + (1=2) \frac{p}{3} \frac{\bar{s}}{s} \sin \theta_{21} \sin \theta_{31} + \sin \theta_{32} ; \\
P(B \rightarrow A) &= \frac{2^h}{9} \sin^2 \frac{21}{2} + 1 + \frac{p}{3} \frac{\bar{c}}{c} \sin^2 \frac{31}{2} + 1 + \frac{p}{3} \frac{\bar{c}}{c} \sin^2 \frac{32}{2} \\
&\quad + (1=2) \frac{p}{3} \frac{\bar{s}}{s} \sin \theta_{21} \sin \theta_{31} + \sin \theta_{32} ; \\
P(B \rightarrow B) &= 1 - P(B \rightarrow C) - P(B \rightarrow A); \\
P(C \rightarrow A) &= \frac{2^h}{9} \sin^2 \frac{21}{2} + 1 + \frac{p}{3} \frac{\bar{c}}{c} \sin^2 \frac{31}{2} + 1 + \frac{p}{3} \frac{\bar{c}}{c} \sin^2 \frac{32}{2} \\
&\quad + (1=2) \frac{p}{3} \frac{\bar{s}}{s} \sin \theta_{21} \sin \theta_{31} + \sin \theta_{32} ; \\
P(C \rightarrow B) &= \frac{2^h}{9} (1=2) \frac{\bar{s}}{s} \sin^2 \frac{21}{2} + \sin^2 \frac{31}{2} + \sin^2 \frac{32}{2} \\
&\quad + (1=2) \frac{p}{3} \frac{\bar{s}}{s} \sin \theta_{21} \sin \theta_{31} + \sin \theta_{32} ; \\
P(C \rightarrow C) &= 1 - P(C \rightarrow A) - P(C \rightarrow B); \tag{4.1}
\end{aligned}$$

with $s = \sin$, $c = \cos$, and

$$f_{fg} = b_0^{(f)} - b_0^{(g)} \frac{L}{\sim c} : \tag{4.2}$$

Specifically, the Fermi point-splitting Ansatz gives

$$\theta_{21} = 2 \theta_{1l} = B_0 L = (\sim c) ; \quad \theta_{32} = 2 \theta_{1r} ; \quad \theta_{31} = 2 \theta_{1l} (1 + r) ; \tag{4.3}$$

in terms of parameters B_0 and r from Eq. (3.3).

The probabilities for right-handed antineutrinos are given by

$$P(X \rightarrow Y; \theta) = P(X \rightarrow Y; \theta) ; \tag{4.4}$$

as follows by changing $\theta \rightarrow \pi - \theta$ and $B_0 \rightarrow -B_0$ in Eq. (4.1), where the latter transformation corresponds to the change from (2.3) to (2.4) with $\theta = \pi$. Note that the survival probability of right-handed antineutrinos equals that of left-handed neutrinos,

$$P(\bar{\nu} \rightarrow \bar{\nu}) = P(\nu \rightarrow \nu); \quad (4.5)$$

independent of the choice of θ in the antineutrino dispersion law (2.4).

The time-reversal asymmetry for the oscillation probabilities between A-type and C-type neutrinos is defined by:

$$a_{CA}^{(T)} = \frac{P(A \rightarrow C) - P(C \rightarrow A)}{P(A \rightarrow C) + P(C \rightarrow A)}; \quad (4.6)$$

For the model probabilities (4.1), this asymmetry parameter is proportional to $\sin \theta$. The corresponding CP asymmetry,

$$a_{CA}^{(CP)} = \frac{P(C \rightarrow A) - P(A \rightarrow C)}{P(C \rightarrow A) + P(A \rightarrow C)}; \quad (4.7)$$

vanishes for $\theta = 1$ and equals $a_{CA}^{(T)}$ for $\theta = -1$. In other words, the oscillation probabilities (4.1) of the neutrino model with $\sin \theta \neq 0$ violate T and CPT for the case of $\theta = 1$ and violate T and CP (but keep CPT invariance intact) for the case of $\theta = -1$. In the absence of a definitive theory, it is up to experiment to decide between the options $\theta = \pm 1$.

Finally, we mention that the standard mass-difference mechanism gives the following oscillation probabilities [17, 18] for fixed ratio $L=E$ and small enough $|m_{21}^2|, |m_{12}^2|, |m_{13}^2|$:

$$P_{\text{mass oscill}}(\nu_e \rightarrow \nu_e) = \sin^2(2\theta_{13}) \sin^2\theta_{32} \sin^2\frac{\pi L}{4L}; \quad (4.8a)$$

$$P_{\text{mass oscill}}(\nu_e \rightarrow \nu_\mu) = \cos^4\theta_{13} \sin^2(2\theta_{32}) \sin^2\frac{\pi L}{4L}; \quad (4.8b)$$

with $\theta_{32} = \frac{m_{21}^2}{m_{32}^2} \frac{c^4 L}{4E} \sim c$. The mixing angles θ_{ij} are related to the mass terms in the action and are, in general, different from those defined by Eqs. (3.1)-(3.2); cf. Ref. [33]. For $|m_{21}^2|, |m_{12}^2|, |m_{13}^2|$ and considering L to be an average distance, one has effectively

$$P_{\text{mass oscill}}(\nu_e \rightarrow \nu_e) = P_{\text{mass oscill}}(\nu_e \rightarrow \nu_\mu) = \frac{1}{2} (1 + 2 \sin^2(2\theta_{13}) \cos^4\theta_{13} \sin^2(2\theta_{21}) \sin^2\frac{\pi L}{4L}); \quad (4.9)$$

with the θ_{13} and θ_{32} terms averaged over. The expressions (4.8ab) have been used to analyze the data from K2K [4, 5] and the expression (4.9) for the data from KamLAND [6, 7]. In the next section, we will use instead the expressions (4.1)-(4.5) from the simple Fermi-point-splitting model.

V. MODEL PARAMETERS AND PREDICTIONS

In order to make clear predictions, we assume in this article that the neutrino masses are strictly zero. It could, however, be that Eqs. (2.3)-(2.4) are modified by having (small) mass squared terms on their right-hand-sides [cf. Eq. (2.5)], but we do not wish to consider that possibility here.

A . General predictions

The most general prediction of the Fermi-point-splitting mechanism of neutrino oscillations is that the oscillation properties are essentially independent of the neutrino energies. This implies undistorted energy spectra for the reconstructed energies in, for example, the current K2K experiment [4, 5] and the future MINOS experiment [23, 24]. (As argued in Ref. [22], the energy spectra from K2K [4] and KamLAND [6, 7] are certainly suggestive of the mass-difference mechanism but do not rule out the Fermi-point-splitting mechanism yet. The same conclusion holds for the zenith-angle distributions of upward-going muons from SK; cf. Fig. 39 of Ref. [3], which appears to have a relatively large uncertainty on the calculated flux of through-going muons.)

Assuming that the energy splittings (4.2) are responsible for the oscillation results of SK, K2K, and KamLAND (see below), another prediction [22] is that any reactor experiment at $L = \sim 1$ km (cf. Refs. [10, 11, 31]) will have survival probabilities close to 1, at least up to an accuracy of order $(b_0 \sim c)^2 \sim 10^{-4}$ for $b_0 \sim 2 \times 10^{12}$ eV.

Both predictions hold, of course, only if mass term effects from the generalized dispersion law (2.5) are negligible compared to Fermi-point-splitting effects. This corresponds to $m^2 < 10^{-6} \text{ eV}^2 = c^4$ for (anti)neutrino energies in the MeV range. (For larger mass differences, the corresponding mixing angles may need to be small, for example $\theta_{13} < 0.2$ for $|m_{13}^2| \sim 2 \times 10^3 \text{ eV}^2 = c^4$ [10, 11].) As mentioned in the preamble of this section, our model predictions will be for $m^2 = 0$, with mixing angles defined by Eqs. (3.1), (3.2) and (3.4).

B . Preliminary parameter values

We now present model probabilities at three dimensionless distances l which have ratios 250:180:735 corresponding to the baselines of the K2K, KamLAND and MINOS experiments, but, initially, we focus on the first two distances. [The dimensionless distance l has been defined in Eq. (4.3).] In Table I, the model probabilities are calculated starting from an appropriate dimensionless distance \tilde{l} and for a fixed phase $\delta = \pi/4$. The \tilde{l} values are chosen so that the following inequality holds: $P(C \rightarrow C) \geq 65\%$ for $0 \leq l \leq \tilde{l}$.

Fixing the ratio r from Eq. (3.3b) to the value $r=2$, Table II also gives model probabilities for different values of the phase δ , whose range can be restricted to $(\delta = 2; \delta = 2\pi)$ without loss of generality. [The probabilities (4.1) are degenerate under $\delta \rightarrow \delta + \pi$ and $(B; C) \rightarrow (C; B)$.]

The last rows of Tables I and II give the experimental results from K2K [4, 5] and KamLAND [6, 7]. The K2K numbers are deduced from the expected total number of events 80 \pm 6 and the observed numbers of ν_e and $\bar{\nu}_e$ events, respectively 56 and 1 (background?). The latest KamLAND value for the average ν_e survival probability is 0.686 ± 0.044 (stat) ± 0.045 (syst).

Regarding the comparison of the model values and the K2K data in Table I, recall that the

normalized Poisson distribution $p(n; \mu) = \frac{\exp(-\mu) \mu^n}{n!}$ gives $p(1;6) \approx 1\%$ and $p(1;3) \approx 15\%$. This suggests that the best value for r is somewhere between 1=8 and 2. Similarly, Table II shows a preference for a value of μ around 4 (or 5=4 with trivial relabelings).

Identifying the Γ value of one particular row in Table I or II with the K2K baseline of 250 km, determines the value of the fundamental energy-difference scale B_0 of the model; cf. Eq. (4.3). Specifically, one has

$$B_0 = \hbar c \frac{1}{L_{K2K}} = 1.04 \cdot 10^{12} \text{ eV} \cdot \frac{250 \text{ km}}{L_{K2K}} \cdot \frac{\Gamma}{0.210} : \quad (5.1)$$

From the numbers in Tables I and II, the combined K2K and KamLAND results then give the following "central values" for the parameters of the model (3.1)–(3.4):

$$B_0 \approx 10^{12} \text{ eV} ; r \approx 1=2 ; \mu \approx 4 \text{ (mod } 5); \quad (5.2)$$

with the identifications

$$\mathcal{A}i = j_e i; \mathcal{B}i = j_i i; \mathcal{C}i = j_i i \quad \mu=4; \quad (5.3a)$$

$$\mathcal{A}i = j_e i; \mathcal{B}i = j_i i; \mathcal{C}i = j_i i \quad \mu=5=4: \quad (5.3b)$$

Only interactions can distinguish between the options (5.3ab). If, for example, the flavor states $\mathcal{A}i$ and $\mathcal{C}i$ appear in decay, one would have $\mu=4$. If, on the other hand, the flavor states $\mathcal{A}i$ and $\mathcal{B}i$ appear, one would have $\mu=5=4$. Henceforth, we focus on the $\mu=4$ case, but our conclusions are independent of this choice.

C. Specific predictions

In order to prepare for the discussion of future experiments, we give in Figs. 1–3 the $\mu=4$ probabilities $P(\mathcal{C} \rightarrow X)$ and $P(\mathcal{A} \rightarrow X)$ as a function of travel distance L . The probabilities $P(\mathcal{B} \rightarrow X)$ equal $1 - P(\mathcal{C} \rightarrow X) - P(\mathcal{A} \rightarrow X)$ and are given in Fig 4. These probabilities $P(\mathcal{B} \rightarrow X)$ are, of course, of less direct experimental relevance if $\mathcal{B}i = j_i i$ as suggested by the identifications (5.3a).

Figures 1–4 give the neutrino oscillation probabilities for the phase $\mu=4$ but the same curves hold for $\mu=5=4$ if the labels B and C are switched. Figure 4, for example, gives the $\mu=5=4$ probabilities $P(\mathcal{C} \rightarrow \mathcal{C})$ [broken curve] and $P(\mathcal{C} \rightarrow \mathcal{B})$ [solid curve]. In the same way, Figs. 1–3 give the $\mu=5=4$ probabilities $P(\mathcal{B} \rightarrow \mathcal{B})$ and $P(\mathcal{B} \rightarrow \mathcal{A})$ [top panels] and $P(\mathcal{A} \rightarrow \mathcal{A})$ and $P(\mathcal{A} \rightarrow \mathcal{B})$ [middle panels].

At this point, we can mention that the model probabilities (4.1) for parameters (5.2)–(5.3) more or less fit the latest L=E distribution from SK [2]. A first model estimate for atmospheric-like events (normalized to the expected numbers without neutrino oscillations) shows, in fact, a "dip" down to some 45% at L=E values just under $10^3 \text{ km} = G \text{ eV}$

and a "plateau" at the 60% level for larger $L=E$ values, which roughly agrees with the experimental data (cf. Fig. 4 of Ref. [2]). The same calculation gives for the normalized distribution of atmospheric ν_e -like events an average value of 1 with a clear dip at $L=E$ values of a few hundred km \approx GeV (cf. Fig. 37 of Ref. [3]). Both dips can be understood heuristically from the relevant curves in Fig. 2, but a reliable model calculation requires further details on the events and experimental cuts.

We now turn to the predictions from the simple Fermi-point-splitting model (3.1)-(3.4) for future experiments. For comparison, we show in the last row of Table I possible results for MINOS from mass-difference neutrino oscillations. Since K2K and MINOS (in the low-energy mode) have a similar $L=E$ ratio, the mass-difference mechanism for neutrino oscillations (4.8) predicts more or less equal probabilities. For the Fermi-point-splitting mechanism, only the travel distance L enters and different probabilities may be expected in general. This is borne out by the model values shown in the last column of Table I.

According to Table I, the allowed range of r values from K2K and KamLAND is rather large, roughly between 1 to 1=4. MINOS, on the other hand, would allow for a more precise determination of r , assuming that the simple model has any validity at all. Figure 5 [top panel] gives the model values for the $\theta = 45^\circ$ (mod) probabilities $P(\nu_\mu \rightarrow \nu_\mu)$ [solid curves] and $P(\nu_\mu \rightarrow \nu_e)$ [broken curves] as a function of r . These probabilities are evaluated at a distance $L = 735$ km corresponding to the MINOS baseline (735 km), provided L corresponds to the K2K baseline (250 km) where $P(\nu_\mu \rightarrow \nu_\mu)$ has been measured to be approximately 0.70 \pm 0.05 [4].

The simple model already makes the prediction that the appearance probability $P(\nu_\mu \rightarrow \nu_e)$ for MINOS could be of the order of 10% or more (see Fig. 5, top panel). This is substantially above the expectations from the mass-difference mechanism which predicts $P(\nu_\mu \rightarrow \nu_e)$ of the order of a few percent at most, based on the stringent upper limits for θ_{13} from CHOOZ [10] and Palo Verde [11].

It is also clear from Fig. 5 [top panel] that a measurement of the survival probability $P(\nu_\mu \rightarrow \nu_\mu)$ by MINOS would allow for a better determination of the value of r in the model, especially if combined with improved measurements of the same probability at $L = 250$ - 295 km from K2K [4, 5] and JPARC (SK) [25]. Indeed, the precise determination of $P(\nu_\mu \rightarrow \nu_\mu)$ at $L = 250$ km would effectively collapse the bands in the top panel of Fig. 5. Assuming a measured value of 0.70 for $P(\nu_\mu \rightarrow \nu_\mu)$ at $L = 250$ km, the variation with r around a value of $\theta = 45^\circ$ (mod) is shown in Fig. 5 [bottom panel]. If MINOS would then measure $P(\nu_\mu \rightarrow \nu_e)$ between 10% and 40%, the further measurement of $P(\nu_\mu \rightarrow \nu_e)$ could be used to constrain the value of r .

Even for the large mixing angle θ_{13} of the simple model (3.1)-(3.4), the probability $P(\nu_\mu \rightarrow \nu_e)$ can be very low at $L < 0.25$, but for larger values of L the probability becomes substantial (cf. Figs. 1-3). In contrast, mass-difference oscillations (4.8a) with a rather small θ_{13} value [10, 11] would have small $P(\nu_\mu \rightarrow \nu_e)$ for all distances L . One of the main objectives of the planned JPARC (SK) experiment (also known as T2K) will be to measure

this appearance probability at $L = 295 \text{ km}$. The relevant model values at $L = 295 = 250$ are given in Fig. 6 [solid curves], together with the values for the time-reversed process [broken curves]. Typical values of $P(\nu_e \rightarrow \nu_e)$ are seen to be around 1%, but lower values are certainly possible [for $\delta_{11} = 32$, the lowest solid curve of the bottom panel drops to zero at $\log r = 0.9426$].

Another quantity of practical importance to future experiments is the wavelength (Table III). In addition, there is the length L_{magic} where the time-reversal asymmetry (4.6) peaks, with $P(\nu_e \rightarrow \nu_e)$ significantly less than $P(\nu_e \rightarrow \nu_e)$. Table III gives the numerical values for this length and the corresponding asymmetry $a_e^{(T)}$. Remarkably, the value of L_{magic} is only weakly dependent on the parameters r and δ_{11} ; see Table III and Fig. 7. The other magic distance is L_{magic}^0 with $P(\nu_e \rightarrow \nu_e)$ significantly larger than $P(\nu_e \rightarrow \nu_e)$. Table III shows that the L_{magic}^0 value depends rather strongly on r . For these large travel distances, matter effects need to be folded in, but the basic T asymmetry $P(\nu_e \rightarrow \nu_e) - P(\nu_e \rightarrow \nu_e)$ is expected to be unaffected; cf. Refs. [17, 18, 30].

With the identifications (5.3) and even allowing for a large δ_{13} value as in the simple model (3.4), the first distance L_{magic} has a very low probability $P(\nu_e \rightarrow \nu_e)$ and would be at approximately 400 km, which is not very much more than the JPARC {SK baseline of 295 km [25]. If the simple model of this article has any relevance, it would be interesting to have also initial ν_e type neutrinos for the JPARC {SK baseline (possibly from a beta beam [28, 30]).

For model parameters (5.2), the second distance L_{magic}^0 with relatively high probability $P(\nu_e \rightarrow \nu_e)$ would be at approximately 2000 km, which is close to the JPARC {Beijing baseline of 2100 km considered in Ref. [26]. But, as mentioned above, the model parameter r needs to be determined first, in order to be sure of the value of L_{magic}^0 .

VI. OUTLOOK

The future is notoriously difficult to predict. Based on the results of this article, one possible roadmap for nonstandard neutrino oscillations might be the following:

1. Does K2K (or MINOS in the low-energy mode) see an unambiguous distortion of the E spectrum or, better, does MINOS find a significantly larger survival probability $P(\nu_e \rightarrow \nu_e)$ for the high-energy beam ($E_{\text{beam}} = 15 \text{ GeV}$) than for the low-energy beam ($E_{\text{beam}} = 3 \text{ GeV}$)?

If so, mass-difference effects may be more important for neutrino oscillations than Fermi-point splitting, at least for the energies considered.

If not, go to 2.

2. Does MINOS find an appearance probability $P(\nu_e \rightarrow \nu_e)$ at or below a few percent?

If so, the simple Fermi-point-splitting model (3.1) { (3.4) would appear to be inappropriate and δ_{13} might be relatively small (if the Fermi-point-splitting model with

nonmaximal mixing angles fits the data, go to 3).

If not, go to 3.

3. Does the (simple) Fermi-point-splitting model fit the data from K2K, KamLAND, and MINOS with consistent values for θ_{12} , r , and δ ?

If not, change the model or find an entirely different neutrino-oscillation mechanism.

If so, reconsider the future options based on the relevant energy-independent length scales of the Fermi-point-splitting model (cf. Table III and Fig. 7). These future options include JPARC [25, 26], BNL [27], beta beams [28, 30], and neutrino factories [29, 30]. Reactor experiments [31] may also be important to constrain or determine possible mass terms in the generalized dispersion law (2.5) and the additional mixing angles and phases.

The hope is that the first two questions can be answered in part by the final results from K2K and the initial results from MINOS.

ACKNOWLEDGEMENTS

It is a pleasure to thank W. J. Marciano for discussions and C. Kaufhold for help with the figures.

-
- [1] Y. Fukuda et al. [Super-Kamiokande Collaboration], Phys. Rev. Lett. 81, 1562 (1998) [arXiv:hep-ex/9807003].
- [2] Y. Ashie et al. [Super-Kamiokande Collaboration], preprint [arXiv:hep-ex/0404034].
- [3] T. Kajita and Y. Totsuka, Rev. Mod. Phys. 73, 85 (2001).
- [4] M. H. Ahn et al. [K2K Collaboration], Phys. Rev. Lett. 90, 041801 (2003) [arXiv:hep-ex/0212007].
- [5] M. H. Ahn et al. [K2K Collaboration], Phys. Rev. Lett. 93, 051801 (2004) [arXiv:hep-ex/0402017].
- [6] K. Eguchi et al. [KamLAND Collaboration], Phys. Rev. Lett. 90, 021802 (2003) [arXiv:hep-ex/0212021].
- [7] T. Araki et al. [KamLAND Collaboration], preprint [arXiv:hep-ex/0406035].
- [8] Q. R. Ahmad et al. [SNO Collaboration], Phys. Rev. Lett. 89, 011301 (2002) [arXiv:nuclex/0204008].
- [9] S. N. Ahmed et al. [SNO Collaboration], Phys. Rev. Lett. 92, 181301 (2004) [arXiv:nuclex/0309004].
- [10] M. Apollonio et al., Eur. Phys. J. C 27, 331 (2003) [arXiv:hep-ex/0301017].
- [11] F. Boehm et al., Phys. Rev. D 64, 112001 (2001) [arXiv:hep-ex/0107009].

- [12] V.N. Gribov and B. Pontecorvo, Phys. Lett. B 28, 493 (1969).
- [13] S.M. Bilenky and B. Pontecorvo, Phys. Lett. B 61, 248 (1976).
- [14] B. Kayser, Phys. Rev. D 24, 110 (1981).
- [15] L. Stodolsky, Phys. Rev. D 58, 036006 (1998) [arXiv:hep-ph/9802387].
- [16] H.J. Lipkin, Phys. Lett. B 579, 355 (2004) [arXiv:hep-ph/0304187].
- [17] V. Barger, D. Marfatia, and K. Whisnant, Int. J. Mod. Phys. E 12, 569 (2003) [arXiv:hep-ph/0308123].
- [18] R.D. McKee and P. Vogel, Phys. Rept. 394, 315 (2004) [arXiv:hep-ph/0402025].
- [19] G.E. Volovik, The Universe in a Helium Droplet (Clarendon Press, Oxford, 2003).
- [20] F.R. Klinkhamer and G.E. Volovik, to appear in JETP Lett. [arXiv:cond-mat/0407597].
- [21] F.R. Klinkhamer and G.E. Volovik, preprint [arXiv:hep-th/0403037].
- [22] F.R. Klinkhamer, JETP Lett. 79, 451 (2004) [arXiv:hep-ph/0403285].
- [23] P. Adamson et al. [MINOS Collaboration], The MINOS Detectors Technical Design Report, October 1998, Fermi Lab report NuMI-L-337 [homepage at <http://www-numi.fnal.gov>].
- [24] K. Lang, JHEP Proceedings AHEP-2003/009.
- [25] Y. Itow et al. [JHF Neutrino Working Group], in: Neutrino Oscillations and Their Origin, edited by Y. Suzuki et al. (World Scientific, Singapore, 2003), pp. 239{248 [arXiv:hep-ex/0106019].
- [26] H.S. Chen et al. [LBL Study Group H2B-1 Collaboration], report IHEP-EP-2001-01 [arXiv:hep-ph/0104266]; Y.F. Wang et al. [LBL Study Group H2B-4 Collaboration], Phys. Rev. D 65, 073021 (2002) [arXiv:hep-ph/0111317]; M. Aoki et al., Phys. Rev. D 67, 093004 (2003) [arXiv:hep-ph/0112338].
- [27] M.V. Divan et al., Phys. Rev. D 68, 012002 (2003) [arXiv:hep-ph/0303081].
- [28] P. Zucchelli, Phys. Lett. B 532, 166 (2002).
- [29] S. Geer, Phys. Rev. D 57, 6989 (1998); D 59, 039903 (E) (1999) [arXiv:hep-ph/9712290].
- [30] A. Blondel et al., ECFA/CERN studies of a European neutrino factory complex, report CERN-2004-002 [arXiv:hep-ph/0210192].
- [31] K. Anderson et al., White paper report on using nuclear reactors to search for a value of θ_{13} , [arXiv:hep-ex/0402041].
- [32] D. Colladay and V.A. Kostelecky, Phys. Rev. D 55, 6760 (1997) [arXiv:hep-ph/9703464].
- [33] S. Coleman and S.L. Glashow, Phys. Rev. D 59, 116008 (1999) [arXiv:hep-ph/9812418].
- [34] S.M. Carroll, G.B. Field, and R. Jackiw, Phys. Rev. D 41, 1231 (1990).
- [35] I. Mocioiu and M. Pospelov, Phys. Lett. B 534, 114 (2002) [arXiv:hep-ph/0202160].
- [36] C. Jarlskog, Phys. Rev. Lett. 55, 1039 (1985).

TABLE I: Model probabilities $(P)_{j=1}^{27}$ for different values of the energy-splitting ratio r and dimensionless distance L , with fixed phase $\delta = \pi/4$. The probabilities P are calculated from Eq. (4.1) and are given in percent, with a rounding error of 1. The last row gives the experimental results, with relative errors of the order of 10%, for $(P_{\mu \rightarrow e}; P_{\mu \rightarrow \tau}; P_{\mu \rightarrow \nu})$ at $L = 250$ km from K2K [4, 5] and for $(P_{\mu \rightarrow e}; P_{\mu \rightarrow \tau})$ at $L = 180$ km from KamLAND [6, 7]. Also shown are possible results for MINOS [23] from mass-difference neutrino oscillations, where the values for $(P_{\mu \rightarrow e}; P_{\mu \rightarrow \tau}; P_{\mu \rightarrow \nu})$ are from Eq. (4.8) for $L = 735$ km, $E = 3$ GeV, $\tan^2 \theta_{12} = 2 \cdot 10^{-3}$, $\sin^2(2\theta_{32}) = 1$, and $\sin^2(2\theta_{13}) = 0.2$.

r	L	$P_{\mu \rightarrow e}; P_{\mu \rightarrow \tau}; P_{\mu \rightarrow \nu}$ $r = 4; \pi$	$P_{\mu \rightarrow e}$ $r = 4; \pi$ $L = 180 = 250$	$P_{\mu \rightarrow e}; P_{\mu \rightarrow \tau}; P_{\mu \rightarrow \nu}$ $r = 4; \pi$ $L = 735 = 250$
1/8	0.250	(75, 6, 19)	(71)	(74, 9, 17)
1/8	0.320	(65, 7, 28)	(57)	(89, 8, 3)
1/4	0.230	(75, 3, 22)	(72)	(58, 17, 25)
1/4	0.260	(70, 3, 27)	(65)	(64, 23, 13)
1/4	0.290	(65, 3, 32)	(59)	(66, 26, 8)
1/2	0.190	(75, 1, 24)	(74)	(27, 29, 44)
1/2	0.210	(70, 1, 29)	(69)	(26, 43, 31)
1/2	0.230	(65, 1, 34)	(64)	(25, 56, 19)
1	0.130	(75, 2, 23)	(79)	(6, 28, 66)
1	0.145	(70, 2, 28)	(74)	(2, 44, 54)
1	0.160	(65, 2, 33)	(69)	(1, 61, 38)
2	0.080	(74, 6, 20)	(81)	(5, 27, 68)
2	0.095	(65, 7, 28)	(74)	(10, 40, 50)
{	{	K2K : (70, < 1, 29)	KamLAND : (69)	MINOS : (67?, 3?, 30?)

TABLE II: Model probabilities $(P)_{j \neq i}^{\tau}$ for different values of the phase δ and dimensionless distance l , with fixed energy-splitting ratio $r = 1/2$. The probabilities P are calculated from Eq. (4.1) and are given in percent, with a rounding error of 1. For different values of δ , $fX;Y;Z$ g stands for a permutation of the basic flavors $fA;B;C$ g. The last line gives the experimental results from K2K and KamLAND; see the caption of Table I for further details.

δ	l	$fX;Y;Z$ g	$P_{X \rightarrow X}; P_{X \rightarrow Y}; P_{X \rightarrow Z}$ τ	$P_{Y \rightarrow Y}$ $\tau_{180=250}$
$\neq 4$	0.135	$fA;C;B$ g	(75, 1, 24)	(92)
$\neq 4$	0.160	$fA;C;B$ g	(66, 1, 33)	(90)
0	0.135	$fA;C;B$ g	(75, 1, 24)	(96)
0	0.160	$fA;C;B$ g	(66, 1, 33)	(94)
+	$\neq 4$	$fC;A;B$ g	(75, 1, 24)	(74)
+	$\neq 4$	$fC;A;B$ g	(65, 1, 34)	(64)
+	$\neq 2$	$fC;A;B$ g ^a	(75, 9, 16)	(86)
+	$\neq 2$	$fC;A;B$ g ^a	(66, 11, 23)	(81)
{ { {			K2K : (70, < 1, 29)	KamLAND : (69)

^a Permutations $fA;B;C$ g and $fB;C;A$ g give the same probabilities.

TABLE III: Length scales for selected model parameters B_0 , r , and δ . With these parameters and identifications (5.3), the model (3.1)–(3.4) gives $P(\nu_\mu \rightarrow \nu_\mu) = 0.70$ at $L = 250$ km; cf. Table I and Eq. (5.1). An arbitrary distance L is made dimensionless by defining $l = B_0 L / (\hbar c)$, in terms of the fundamental energy-difference scale B_0 . Shown are the (dimensionless) wavelength (l_{wave}), the (dimensionless) magic distance (l_{magic}) L_{magic} which maximizes the time-reversal asymmetry $a_e^{(\tau)}$ for ν_e type and $\bar{\nu}_e$ type neutrinos as defined by Eq. (4.6), and the magic distance L_{magic}^0 which minimizes the asymmetry (cf. Figs. 1–3).

B_0 [10^{-12} eV]	r	(mod.)	l_{wave}	[km]	l_{magic}	L_{magic} [km]	$a_e^{(\tau)}(L_{\text{magic}})$	L_{magic}^0 [km]
0.72	1	$\neq 4$	1	1724	0.224	386	+ 89 %	1338
1.04	1/2	$\neq 4$	2	2381	0.300	357	+ 99 %	2024
1.29	1/4	$\neq 4$	4	3846	0.411	395	+ 81 %	3451

$$\delta = \pi/4, r = 1$$

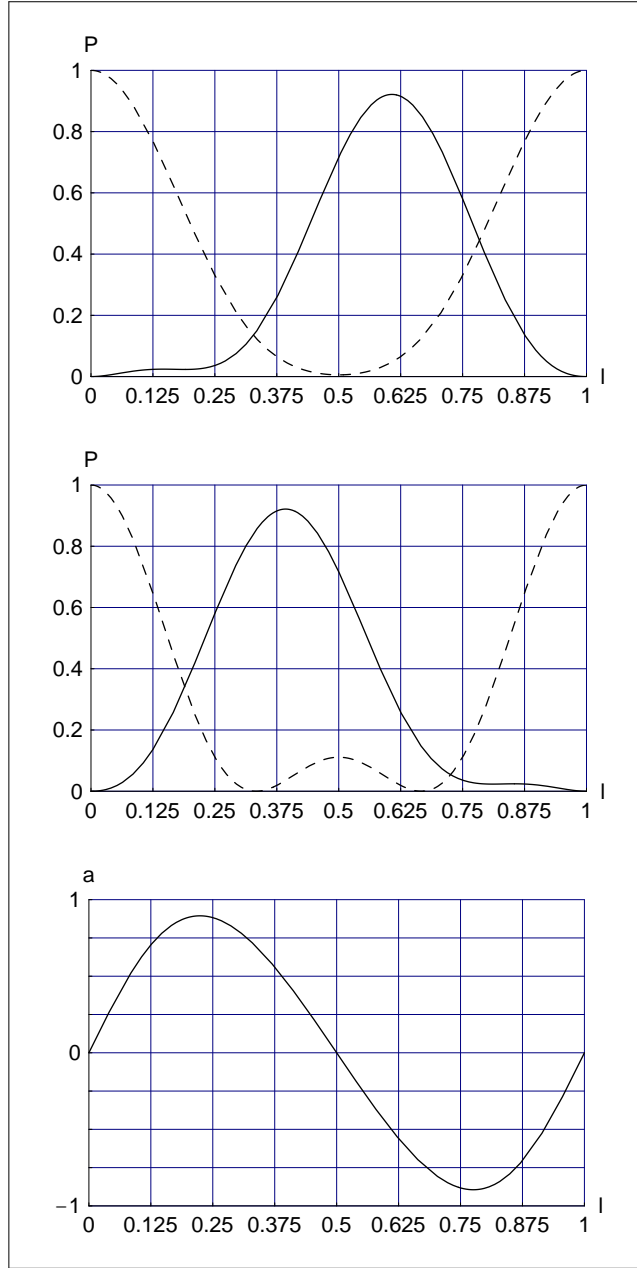


FIG. 1: Model probabilities for vacuum neutrino oscillations as a function of the dimensionless distance l . The probabilities P are calculated from Eq. (4.1), with phase $\delta = \pi/4$ and energy-splitting ratio $r = 1$. The top panel shows $P(C \rightarrow C)$ [broken curve] and $P(C \rightarrow A)$ [solid curve], with $P(C \rightarrow B) = 1 - P(C \rightarrow C) - P(C \rightarrow A)$. The middle panel shows $P(A \rightarrow A)$ [broken curve] and $P(A \rightarrow C)$ [solid curve], with $P(A \rightarrow B) = 1 - P(A \rightarrow A) - P(A \rightarrow C)$. The bottom panel gives the time-reversal asymmetry (4.6) for oscillations between A type and C type neutrinos. Based on the comparison with the K2K data for flavor identifications $\bar{\nu}_\mu \rightarrow \bar{\nu}_\mu$ and $\bar{\nu}_\mu \rightarrow \bar{\nu}_\tau$, the wavelength $l = 1$ would correspond to approximately 1700 km (cf. Table III).

$$\delta = \pi/4, r = 1/2$$

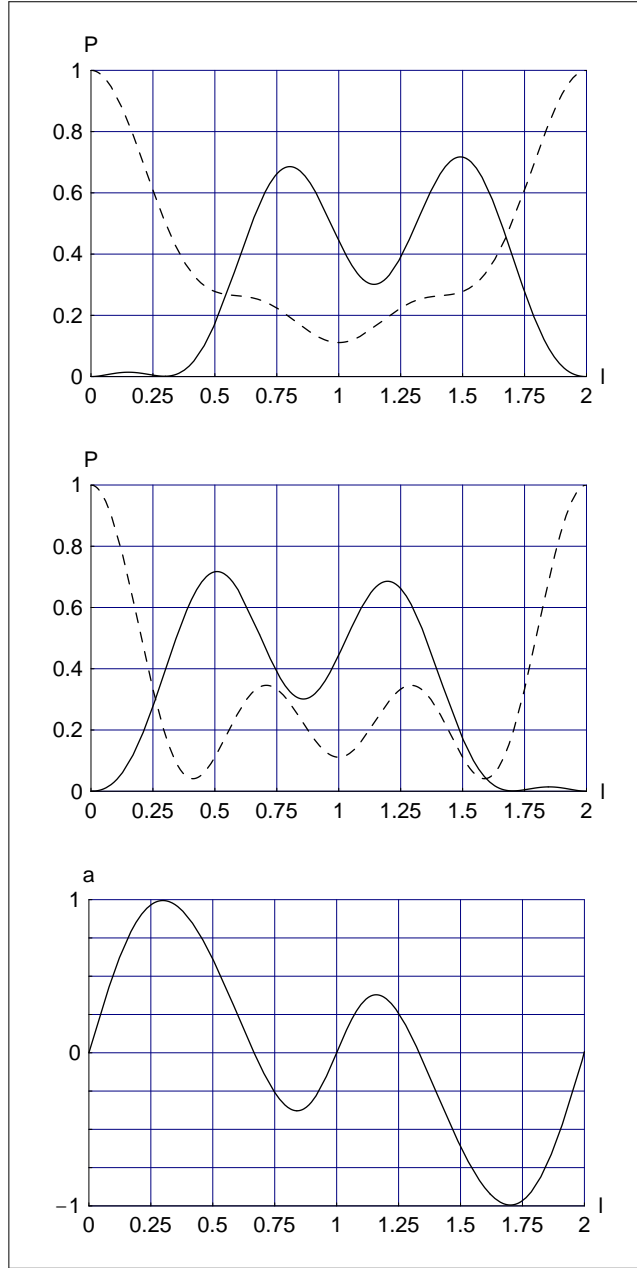


FIG . 2: Same as Fig. 1 but for the energy-splitting ratio $r = 1/2$. The wavelength $l = 2$ would correspond to approximately 2400 km , according to Table III.

$$\delta = \pi/4, r = 1/4$$

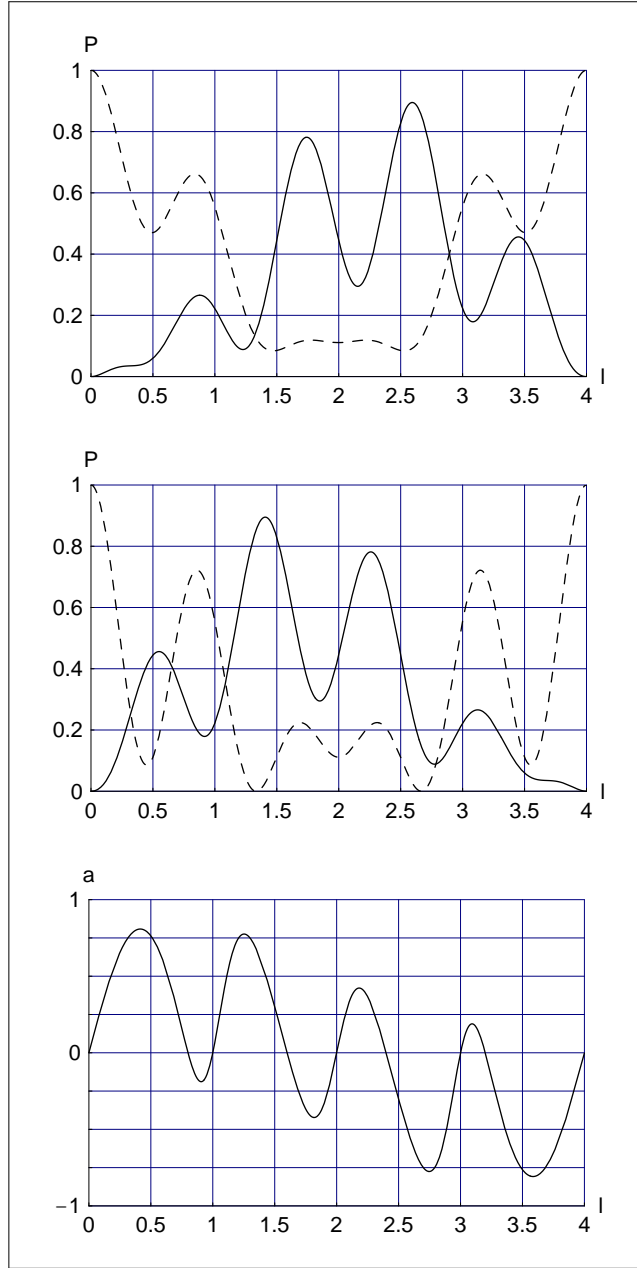


FIG . 3: Same as Fig. 1 but for the energy-splitting ratio $r = 1/4$. The wavelength $l = 4$ would correspond to approximately 3800 km, according to Table III.

$$\delta = \pi/4$$

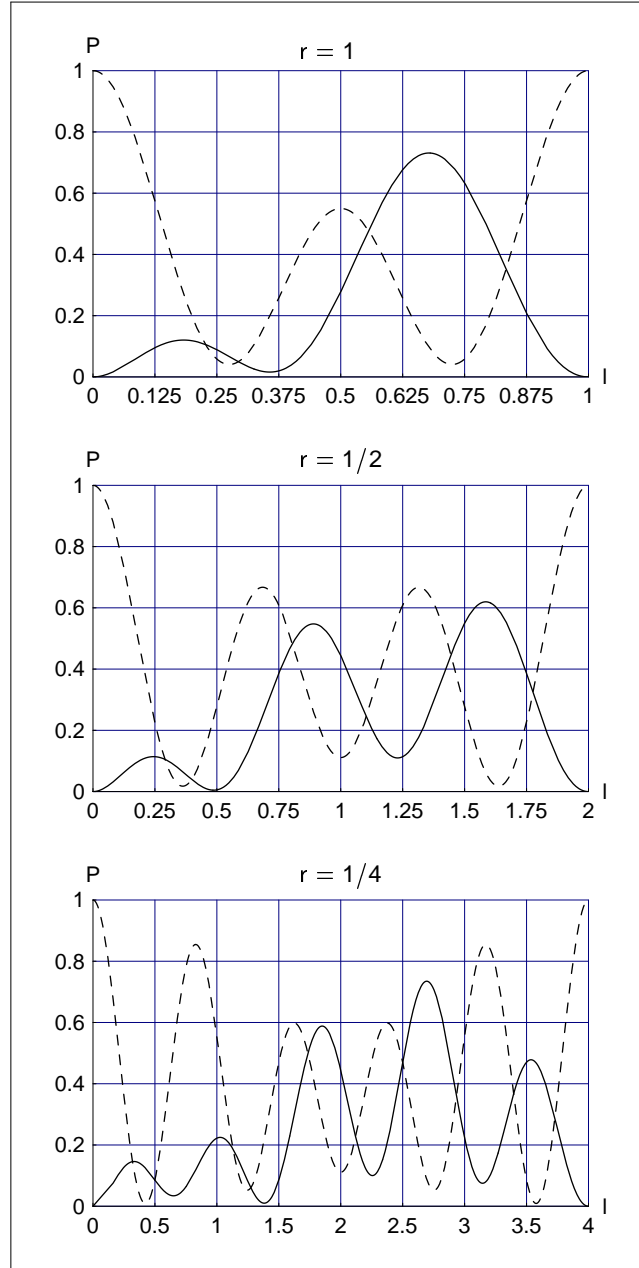


FIG. 4: Model probabilities $P(B \rightarrow B)$ [broken curve] and $P(B \rightarrow C)$ [solid curve] as a function of the dimensionless distance l , with fixed phase $\delta = \pi/4$ and different energy-splitting ratios r . These probabilities are calculated from Eq. (4.1) and $P(B \rightarrow A)$ is given by $1 - P(B \rightarrow B) - P(B \rightarrow C)$. The flavor identifications from Eq. (5.3a) would be $\beta_i = j_i$ and $\bar{\beta}_i = \bar{j}_i$ and, according to Table III, the wavelengths for $r = 1; 1/2$, and $1/4$ would correspond to some 1700, 2400, and 3800 km, respectively.

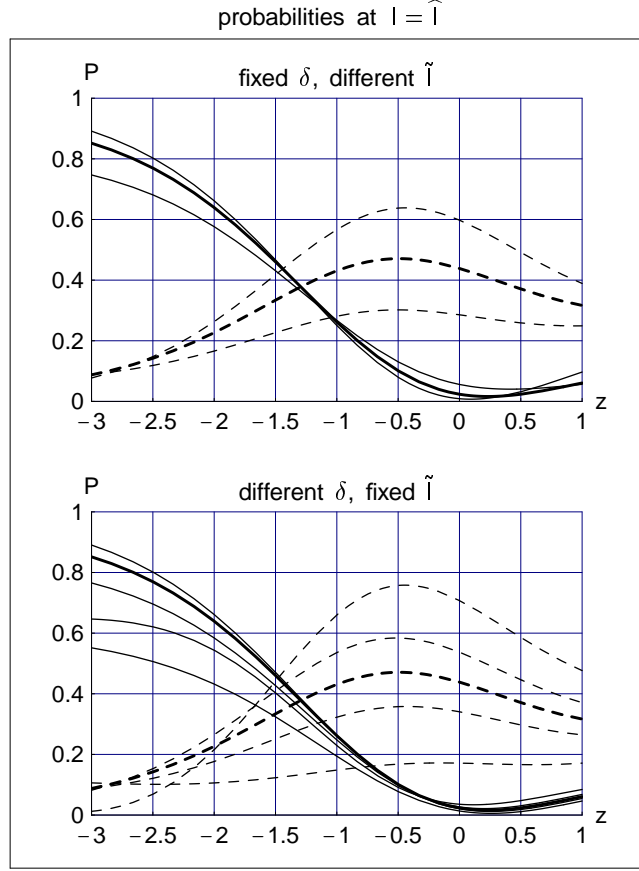


FIG. 5: Model probabilities $P(\delta, \tilde{l})$ [solid curves] and $P(\delta_e, \tilde{l})$ [broken curves] as a function of parameter $z = \log_2 r$, evaluated at the dimensionless distance $\tilde{l} = 735/250$ and with flavor identifications (5.3). The curves of the top panel have phase $\delta = -4 \pmod{32}$ and \tilde{l} defined as the smallest distance for which $P(\delta, \tilde{l}) = 0.70 \pm 0.05$ [the central value 0.70 corresponding to the heavy lines]. Specifically for the top panel, the broken lines at $z = 1$ and the solid lines at $z = -3$, both from top to bottom, have $P(\delta, \tilde{l})[\tilde{l}] = 0.65; 0.70; 0.75$, respectively. The curves of the bottom panel have length \tilde{l} defined as the smallest distance for which $P(\delta, \tilde{l}) = 0.70$ and phase $\delta = 5 \pmod{32}; 7 \pmod{32}; -4 \pmod{32}; 9 \pmod{32}; 11 \pmod{32}$ [the central value $-4 \pmod{32}$ corresponding to the heavy lines]. Specifically for the bottom panel, the broken lines at $z = 1$ from top to bottom have $\delta = 5; 7; 8; 9; 11$, respectively, and the solid lines at $z = -3$ from top to bottom have $\delta = 7; 8; 9; 5; 11$, respectively. The curves of this figure, with \tilde{l} corresponding to the K2K baseline of 250 km, may be relevant to the forthcoming MINOS experiment with a baseline of 735 km.

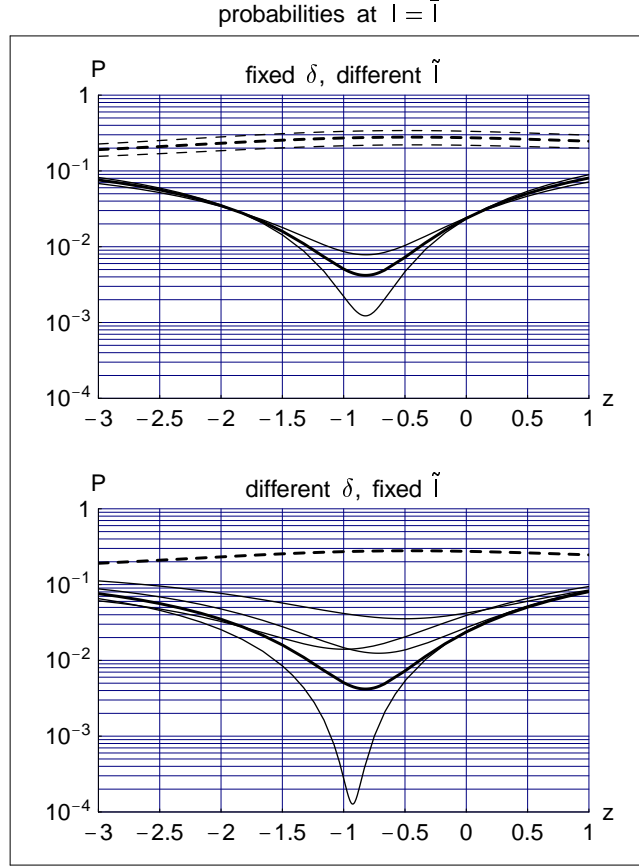


FIG. 6: Model probabilities $P(\nu_e \rightarrow \nu_e)$ [solid curves] and $P(\nu_e \rightarrow \nu_\mu)$ [broken curves] as a function of parameter $z = \log_2 r$, evaluated at the dimensionless distance $l = \tilde{l} = 295 = 250$ and with flavor identifications (5.3). The curves of the top panel have phase $\delta = \pi/4 \pmod{\pi}$ and \tilde{l} defined as the smallest distance for which $P(\nu_e \rightarrow \nu_e) = 0.70 \pm 0.05$ [the central value 0.70 corresponding to the heavy lines]. Specifically for the top panel, the solid lines from top to bottom and the broken lines from bottom to top, both at $z = -1$, have $P(\nu_e \rightarrow \nu_e)[\tilde{l}] = 0.75; 0.70; 0.65$, respectively. The curves of the bottom panel have length \tilde{l} defined as the smallest distance for which $P(\nu_e \rightarrow \nu_e) = 0.70$ and phase $\delta = \pi/32; 7\pi/32; \pi/4; 9\pi/32; 11\pi/32 \pmod{\pi}$ [the central value $\pi/4 \pmod{\pi}$ corresponding to the heavy lines]. Specifically for the bottom panel, the solid lines at $z = 0.5$ from top to bottom have $\delta = \pi/32; \pi/5; \pi/9; \pi/8; \pi/7$, respectively, whereas the broken lines have a rather narrow band on this logarithmic plot and only the heavy broken line for $\delta = \pi/4 \pmod{\pi}$ is shown. The solid curves of this figure, with \tilde{l} corresponding to the K2K baseline of 250 km, may be relevant to the planned JPARC ν SK experiment with a baseline of 295 km.

time-reversal asymmetry: different δ

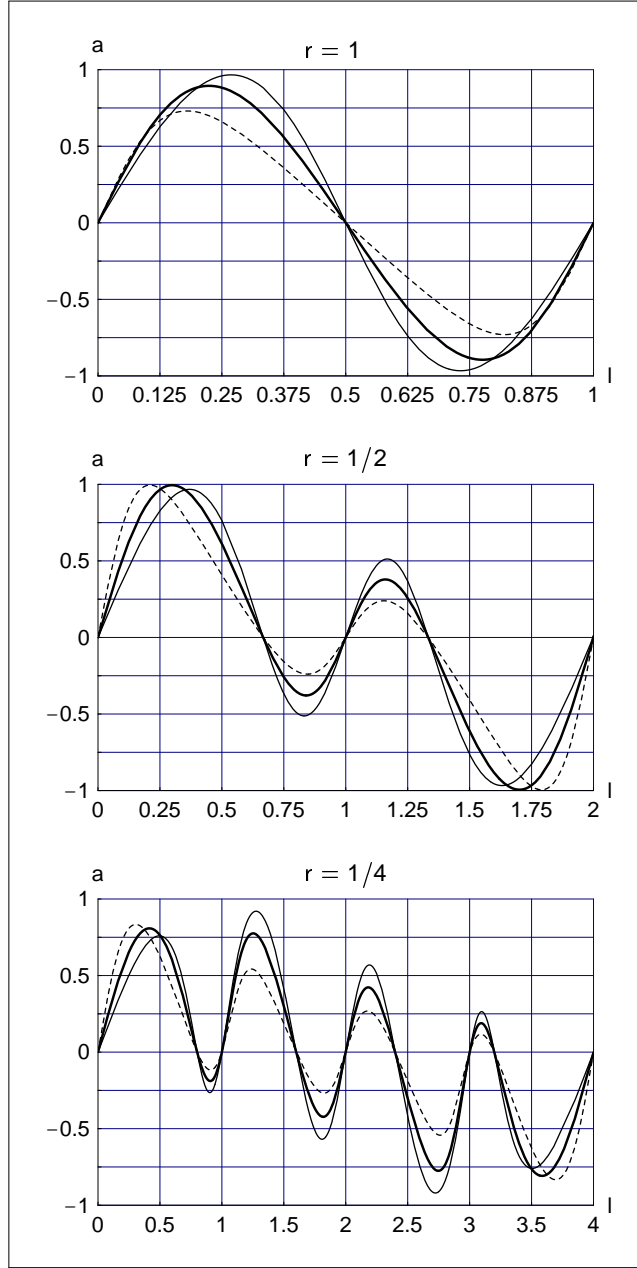


FIG. 7: Model predictions for the time-reversal asymmetry (4.6) of vacuum oscillations between e -type and μ -type neutrinos for different values of the energy-splitting ratio r and different values of the phase, $\delta = 5^\circ, 32^\circ, 4^\circ, 11^\circ, 32^\circ \pmod{360^\circ}$ [the central value $\delta = 4^\circ \pmod{360^\circ}$ corresponding to the heavy lines, the low value to the broken lines, and the high value to the thin lines]. The probabilities entering the asymmetry parameter a are calculated from Eq. (4.1) and the flavor identifications are given by Eq. (5.3). According to Table III, the wavelengths for $r = 1; 1/2$, and $1/4$ would correspond to some 1700, 2400, and 3800 km, respectively.